Arabian Journal of Chemistry (2021) **14**, 103349

King Saud University

Arabian Journal of Chemistry

www.ksu.edu.sa
www.sciencedirect.com

ORIGINAL ARTICLE

Tb_2CoMnO_6 double perovskites nanoparticles as photocatalyst for the degradation of organic dyes: Synthesis and characterization

Mina Dara [a], Mohammad Hassanpour [a], Omid Amiri [b,c], Mahin Baladi [a], Masoud Salavati-Niasari [a,*]

[a] *Institute of Nano Science and Nano Technology, University of Kashan, Kashan, P.O. Box 87317-51167, Iran*
[b] *Faculty of Chemistry, Razi University, Kermanshah 6714414971, Iran*
[c] *Department of Chemistry, College of Science, University of Raparin, Rania, Kurdistan Region, Iraq*

Received 27 May 2021; accepted 19 July 2021
Available online 4 August 2021

KEYWORDS

Tb_2CoMnO_6;
Double perovskite;
Nanoparticles;
Sol-gel;
Auto-combustion;
Photocatalyst

Abstract The importance of water is so high that new methods and materials are constantly being developed to increase freshwater quality. For this purpose, to investigate the unique properties of double perovskites in the photocatalytic process, novel Tb_2CoMnO_6 nanoparticles were synthesized using the sol-gel auto-combustion method. In this method, maltose, cellulose, and Date syrup were used as fuel. Two different ratios of maltose were tested to investigate the effect of fuel content on size and morphology. The synthesized particles in the presence of maltose in an equal ratio to the precursor were selected as the optimal sample by using different analyses such as X-ray diffraction (XRD) and scanning electron microscopy (SEM). Other properties of optimal nanoparticles were investigated using transmission electron microscopy (TEM), energy dispersive spectrometry (EDS), Fourier transform infrared (FTIR), vibrating sample magnetometer (VSM) and diffuse reflectance analysis (DRS) analysis. These nanoparticles were used to investigate the photocatalytic properties under UV light in the aqueous solution of Eriochrome black T, Rhodamine B, Thymol blue, and Acid red dyes. The results of the photocatalytic process showed 70% discoloration for the Eriochrome Black T. Three compounds, include Ethylenediaminetetraacetic acid, 1,4-Benzoquinone, and Benzoic acid, were used as scavengers to investigate the mechanism of the photocatalytic process. The results showed that the mechanism of the photocatalytic process proceeds through superoxide radicals, which Benzoquinone scavenges.

* Corresponding author.
E-mail address: Salavati@kashanu.ac.ir (M. Salavati-Niasari).
Peer review under responsibility of King Saud University.

Production and hosting by Elsevier

https://doi.org/10.1016/j.arabjc.2021.103349

1. Introduction

Freshwater has long been one of the main problems for human life, and efforts to access water resources have always been ongoing (Iglesias, 2020). Today, humans are facing a decrease in freshwater resources (Natalia et al., 2020). Therefore, finding new and cost-effective solutions for managing, purifying, and reusing water is at the forefront of scientific projects, and progress in these areas is constantly occurring (Gomes et al., 2019; Mukhopadhyay et al., 2020; Chaplin, 2019). The photocatalysis process is one of the most important and valuable methods for water treatment.

The photocatalysis is a process that removes contaminants in water under visible or UV light in the presence of a light-sensitive compound (Al-Mamun et al., 2019). Semiconductors are light-sensitive materials that cause electron-hole pairs in the environment when light hits them due to electron transfer (Zhu and Zhou, 2019). The electron-hole created in the aqueous medium leads to the production of free radicals. The interaction of these free radicals with water pollution causes their removal (Koe et al., 2020). Semiconductor materials include a wide range of compounds. One of these large families is the perovskites (Mitzi, 2019).

The structure of perovskite includes a family of materials with different properties and applications (Assirey, 2019). Oxide-type inorganic perovskites are materials of interest for use in many applications, including solar cells, sensors, catalysts, and as anodes in lithium-ion batteries (Jung and Park, 2015; George et al., 2020; Garcia-Muñoz et al., 2019; Chang et al., 2021). From this large family, double perovskites with the structure M_2ABO_6 (M is an element of lanthanides, A, and B of transition metals) have recently attracted the attention of many researchers due to their unique ferromagnetic and optical properties with direct band-gap. Various applications have been reported for these materials, such as La_2NiMnO_6 with application in solar-cell, Gd_2CoMnO_6 with dielectric properties, and La_2MnTiO_6 used as photocatalyst (Sariful Sheikh et al., 2017; Silva et al., 2019; Shirazi et al., 2020). These various properties and applications promise the potential of these materials in different processes.

Various methods, include ultrasonic, sol–gel, and co-precipitation, have been reported in the literature to synthesize double perovskites (Baladi et al., 2019; Dara et al., 2021; Wu et al., 2013). For example, Sivasamy et al. Synthesized Gd_2MnFeO_6 nanoparticles by the sol–gel method, and the optical and magnetic properties of these nanoparticles were investigated (Sivasamy et al., 2020). In this work, the sol–gel auto-combustion method was used for the synthesis of nanoparticles. Tb_2CoMnO_6 double perovskite nanoparticles were synthesized for the first time. Different fuels were used to reach the appropriate size of nanoparticles. For the first time, Date syrup was used as natural fuel for the synthesis of nanoparticles. The ultimate goal was to evaluate the efficiency of these nanoparticles in the photocatalysis process as a potential candidate. The photocatalytic activity of these nanoparticles and the mechanism of the photocatalysis process was investigated for the first time.

2. Experimental

2.1. Material and characterization

All the chemicals used in this work were commercially available and employed without further purification. $Tb(NO_3)_3{\cdot}6H_2O$ with a molecular weight of 453.03 $g.mol^{-1}$, $Mn(NO_3)_2{\cdot}4H_2O$ with a molecular weight of 251.01 $g.mol^{-1}$, $Co(NO_3)_2{\cdot}6H_2O$ with a molecular weight of 291.03 $g.mol^{-1}$ with a purity of over 99% were purchased from Merck company. A diffractometer of the Philips company with X'PertPro monochromatized Cu Kα radiation (λ = 1.54 Å) was used to collect XRD (X-ray diffraction) patterns to confirm the type of structure and check the purity of synthesized nanoparticles. The microscopic morphology of the products was studied by FESEM (field emission scanning electron microscopy) (Mira3 tescan). EDS (energy dispersive spectrometry) analysis was studied by XL30, Philips microscope. Transmission electron microscopy (TEM) image was achieved via a Philips EM208 transmission electron microscope with an accelerating voltage of 200 kV. Fourier transform infrared (FTIR) spectra were detected by means of Nicolet Magna-550 spectrometer in KBr pellets The UV–vis diffuse reflectance analysis was done by applying a UV–vis spectrophotometer (Shimadzu, UV2550, Japan). Magnetic properties were measured using VSM (vibrating sample magnetometer) (Meghnatis. Daghigh Kavir Co.; Iran).

2.2. Synthesis procedure

A sol–gel auto-combustion method with a ratio of 2: 1 Tb $(NO_3)_3{\cdot}6H_2O$ (2 mmol) to $Co(NO_3)_2{\cdot}6H_2O$ (1 mmol) and $Mn(NO_3)_2{\cdot}6H_2O$ (1 mmol) in the presence of maltose, cellulose, and date syrup was used as fuel for the synthesis of Tb_2CoMnO_6 double perovskite nanoparticles. All salts were dissolved separately in distilled water. Fuel dissolved in distilled water was added to the solution containing terbium on the stirrer. The other two solutions containing cobalt and manganese were added to terbium and fuel after mixing. The resulting solution was completely homogenized on a stirrer for 50 min at 50 °C. Then the temperature increased to 110 °C, and after 30 min and combustion, a soft powder was obtained. The resulting powder was calcined at 1000, 900 and 800 °C. Different conditions were adopted for synthesis, as shown in Table 1.

2.3. Photocatalysis tests

The photocatalysis test was performed under UV light to investigate the application of Tb_2CoMnO_6 nanoparticles in the photocatalysis process. For photocatalysis testing, four solutions of Rhodamine B, Eriochrome Black T, Thymol blue, and Acid red dyes with a concentration of 20 ppm were prepared. The total volume of the dye solution was 100 ml. 0.05 gr of Tb_2CoMnO_6 nanoparticles were added as a catalyst to the dye solution. The resulting mixture was aerated for

Table 1 Different conditions of synthesis Tb_2CoMnO_6 double perovskite nanoparticles.

No.	Mole ratio of Tb:Co:Mn	Fuel	Ratio of fuel to Tb	Calcination temperature °C
1	2:1:1	Maltose	1:1	1000
2	2:1:1	Maltose	1:1	900
3	2:1:1	Maltose	1:1	800
4	2:1:1	Cellulose	1:1	800
5	2:1:1	Date syrup	0.5 gr	800
6	2:1:1	Maltose	1:2	800
7	2:1:1	Maltose	3:2	800

20 min in a light-free medium to equilibrate dye adsorption on the catalyst surface. After that, UV light was applied to the mixture. Sampling was performed at specific times, and after centrifugation and catalyst separation, the adsorption of the solution at λ_{max} of dye was analyzed by UV–Vis spectrometer. The efficiency of the photocatalysis process was calculated as follows:

$$\% \text{ Discolorationrization} = (A_0 - A_t)/A_0 \times 100$$

where A_0 and A_t are the absorbance value of dye solution at 0 and t min, respectively (Hassanpour et al., 2021).

3. Results and discussion

In the first step, XRD analysis was used to confirm the formation of Tb_2CoMnO_6 nanoparticles. However, since these nanoparticles were first synthesized, the XRD pattern recorded in the reference was not found. Hence, the XRD patterns obtained were compared with the existing patterns. A recorded pattern for Gd_2CoMnO_6 (JCPDS card number: 01-085-0960) was used to confirm the formation of these nanoparticles. As shown in Fig. 1, the pattern obtained for Tb_2CoMnO_6 nanoparticles is utterly consistent with the reference. This adaptation confirms the orthorhombic phase of Tb_2CoMnO_6 nanoparticles.

The data obtained by X-ray analysis were used to accomplish Rietveld structural refinement to obtain the structural parameters, which was done using FullProf software (Rodríguez-Carvajal, 1993). $TbMnO_3$ structural data was used to perform the Rietveld analysis, which was applied by considering the small difference in the ionic radii of Mn^{3+} (0.58 Å) and Co^{3+} (0.54 Å). Also, the occupation of half of the Mn atom position with Co to achieve the Tb_2CoMnO_6 structure was considered. The result of refined structural parameters in the orthorhombic space group Pbnm were a = 5.312, b = 5.659, c = 7.546 and the reliability factors R_p = 26.7, R_{wp} = 34, R_{exp} = 18.20 and χ^2 = 3.48. X-ray diffraction Rietveld refinement pattern was shown in Fig. 2. XRD analy-

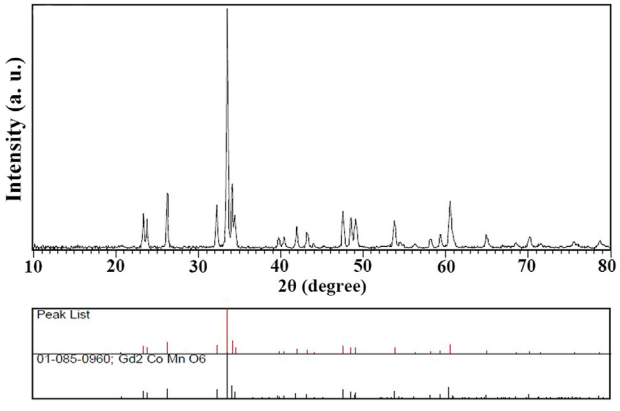

Fig. 1 XRD pattern of synthesized Tb_2CoMnO_6 nanoparticles in the presence of maltose as fuel in comparison with Gd_2CoMnO_6 reference peak.

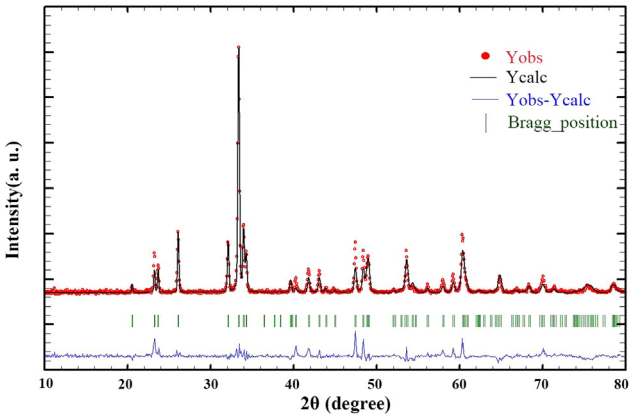

Fig. 2 X-ray diffraction Rietveld refinement patterns of Tb_2CoMnO_6 nanoparticles.

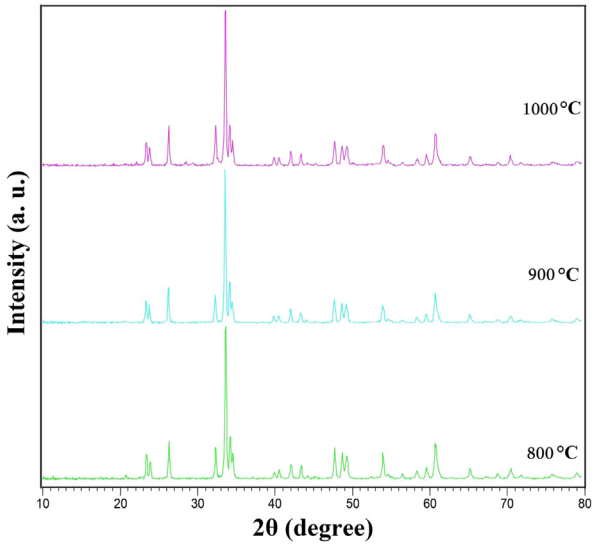

Fig. 3 Patterns obtained from XRD analysis of Tb_2CoMnO_6 nanoparticles prepared in the presence of maltose as fuel at different calcination temperature.

sis was performed on nanoparticles obtained after calcination at three different temperatures, 1000, 900, and 800 °C. It was found that there is not much difference in the patterns by comparing these three patterns (Fig. 3). So the temperature of 800 °C was chosen as the optimal temperature to continue the synthesis of nanoparticles. The crystallite size of the Tb_2CoMnO_6 nanoparticles is obtained to be around 37 nm using the Scherrer equation, $Dc = K\lambda/\beta Cos\theta$ (Hassanpour et al., 2021).

As shown in Table 1, the type and ratio of fuel were investigated to obtain the optimal size and morphology of the nanoparticles. SEM analysis was used to investigate these effects.

The SEM analysis of the effect of different fuels on morphology and particle size was shown in Fig. 4. Three fuels, maltose, cellulose, and Date syrup, were used in this study (Fig. 4 (a), (b), and (c), respectively). The fuel used in the sol–gel method homogenizes the solution by forming a complex with ions and also produces heat, carbon dioxide, and water during the combustion process. Complex formation is actually a type of capping agent that prevents the agglomeration of particles and the formation of by-products. The type of fuel also helps to create better combustion and to form a product with higher purity (Dara et al., 2021; Bhagwat et al., 2019). As is well known, when maltose was used, the particles were smaller in size and wholly monodispersed. However, par-

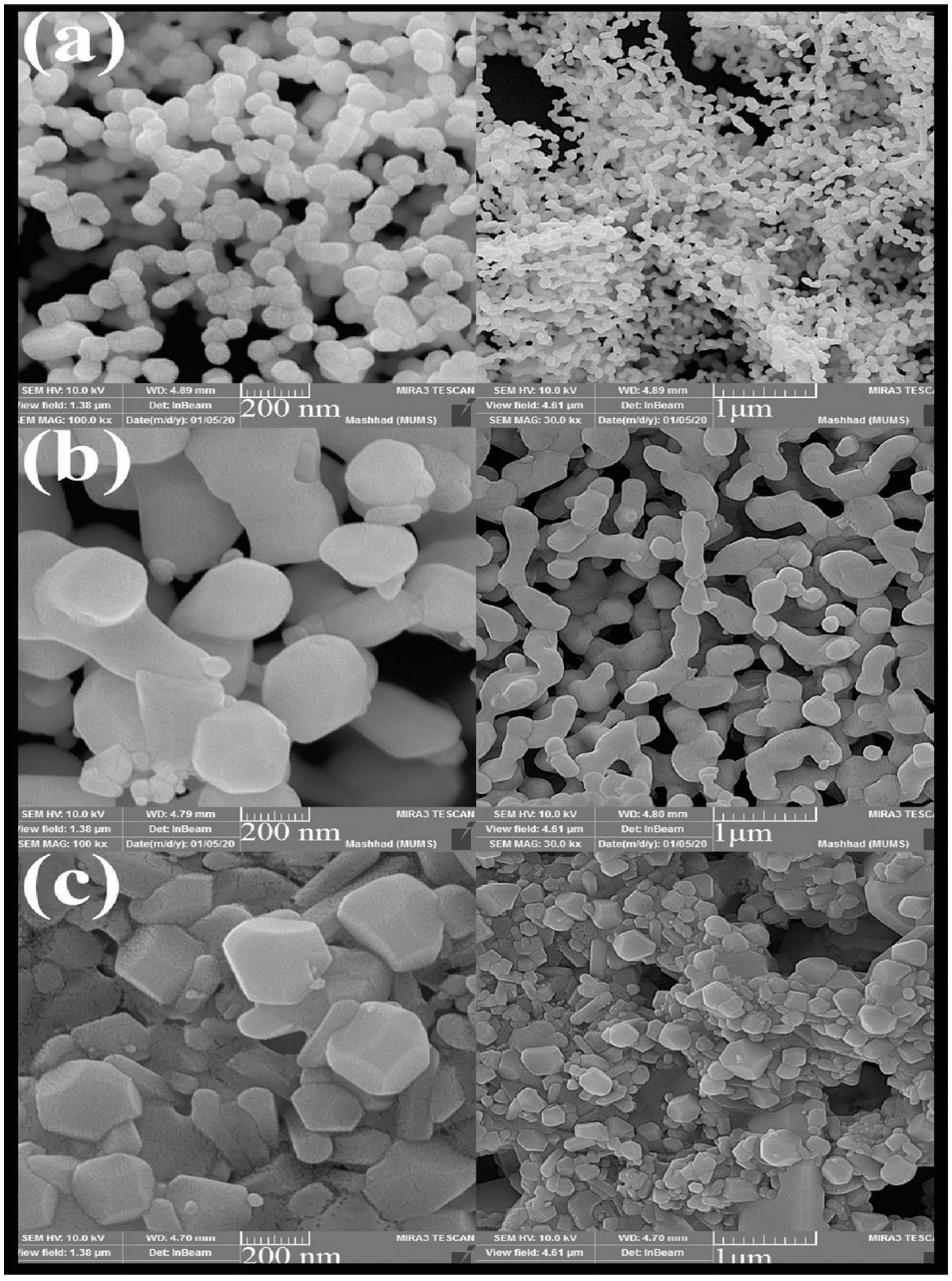

Fig. 4 SEM images of Tb_2CoMnO_6 nanoparticles synthesised in the presence of different fuel (a) Maltose, (b) Cellulose, and (c) Date syrup.

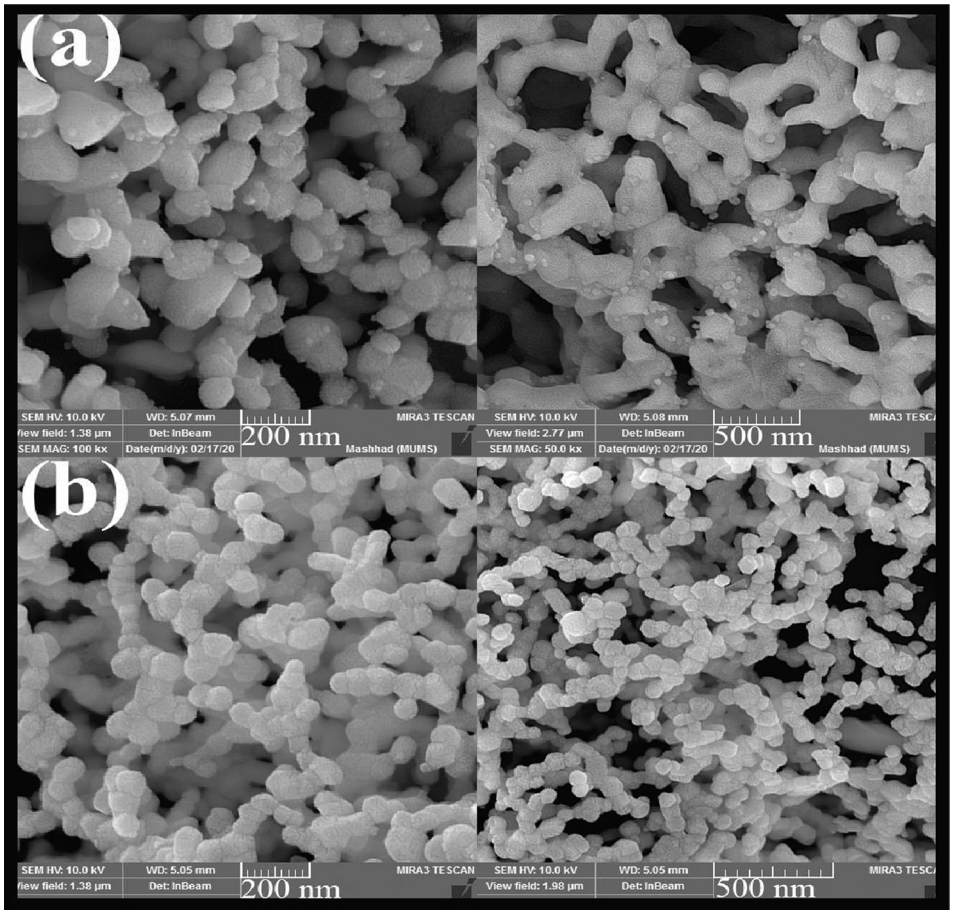

Fig. 5 SEM images of Tb_2CoMnO_6 nanoparticles synthesised in the presence of different ratios of maltose to terbium (a) 1:2 and (b) 3:2.

ticles stuck together in the presence of cellulose and Date syrup. According to these images, maltose was selected as the optimal fuel. The study of the effect of fuel on morphology and particle size was continued by changing the ratio of maltose to terbium precursor. As shown in Fig. 5, when a lower fuel ratio was used to perform the reaction (Fig. 5 (a)), the particles coalesced to form elliptical masses. On the other hand, when higher maltose was applied, obtained particles had smaller and almost spherical sizes (Fig. 5 (b)).

Finally, by examining the images obtained from SEM and considering the results of XRD analysis, the sample prepared in the presence of maltose as fuel with a ratio equal to terbium was selected as the optimal sample in terms of size and morphology (Sample No. 3) and for further investigations were used.

TEM images were used to investigate the morphology of the particles. TEM images obtained from TFMO nanoparticles of sample S3 were shown in Fig. 6. The nanoparticles obtained in the resulting images showed that the nanoparticles are adhered together and agglomerated. Examination of particle size showed particle size in the range of 30 to 40 nm.

EDS analysis was used to confirm the presence of elements in the composition and confirm the absence of impurities in the synthesized Tb_2CoMnO_6 nanoparticles. As shown in Fig. 7, Tb, Co, Mn, and O elements in the obtained spectrum were confirmed. Then, FT-IR analysis was performed for the optimal sample to investigate the intermolecular bonds and confirm the complete removal of the organic compounds used in the synthesis steps. Two peaks at 3442 and 1630 cm^{-1} were observed in the resulting spectrum shown in Fig. 8, which is related to the moisture adsorbed on the surface of the nanoparticles during the sample preparation process for analysis (Hassanpour et al., 2021). The two peaks observed in 595 and 464 cm^{-1} correspond to the metal–oxygen bonds, which can be related to Mn—O and Co—O, respectively (Dara et al., 2021).

One of the essential features for wastewater treatment using nanoparticles is the accessible collection of nanoparticles after the process (Huang et al., 2015). In fact, the importance of the magnetic properties of nanoparticles is highlighted here. Therefore, the magnetic properties of the synthesized nanoparticles (sample No.3) were investigated using VSM analysis. As shown in Fig. 9, a skinny hysteresis loop showed a coercive field of 200 Oe and remnant magnetization of 0.003 $emu.g^{-1}$. These negligible values confirm the paramagnetic behavior of the synthesized nanoparticles.

One of the most important properties in studying the photocatalysis of nanoparticles is their optical properties (Samanta et al., 2018). As mentioned earlier, semiconductor materials with a suitable band-gap are potential options for the photocatalytic process. The value of band-gap plays an essential role in choosing the type of light that is used for irradiation to catalyst. DRS analysis was used to investigate the optical properties of Tb_2CoMnO_6 nanoparticles (sample No. 3). As shown in

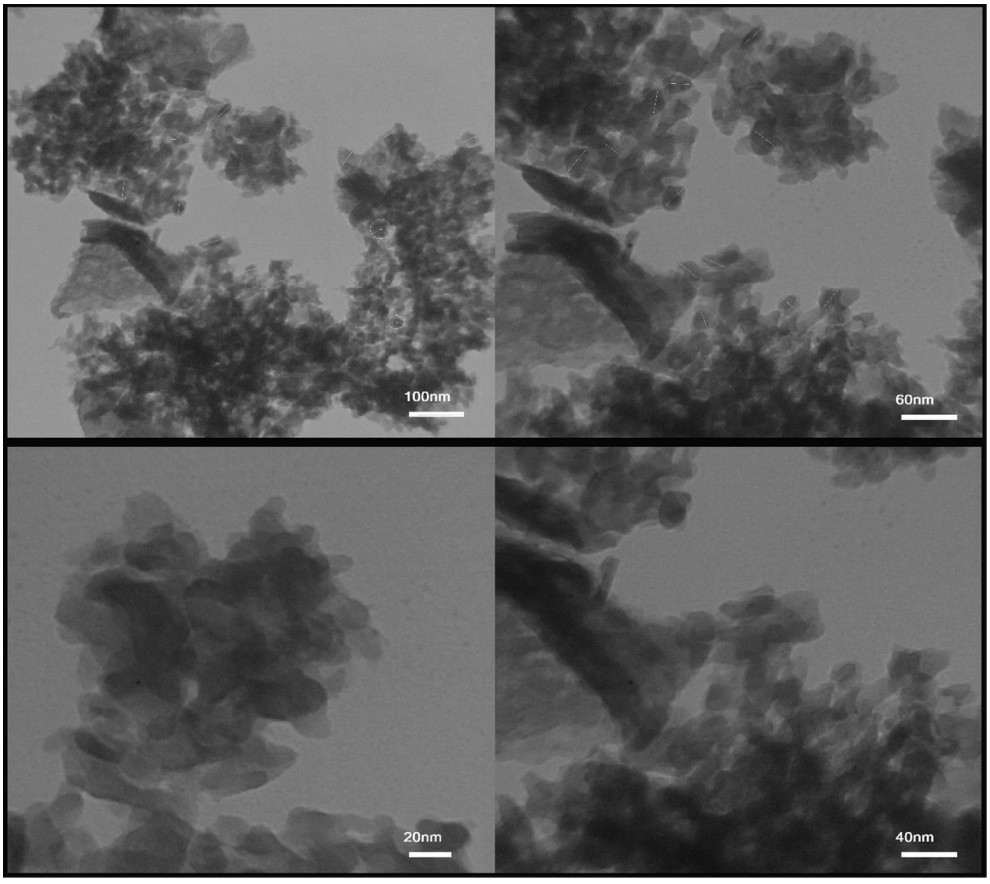

Fig. 6 TEM images obtained from Tb_2CoMnO_6 nanoparticles sample No. 3.

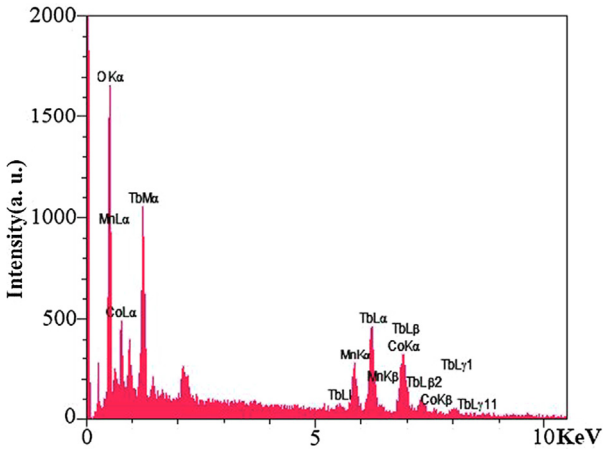

Fig. 7 Results of EDS analysis for Tb_2CoMnO_6 nanoparticles sample No. 3.

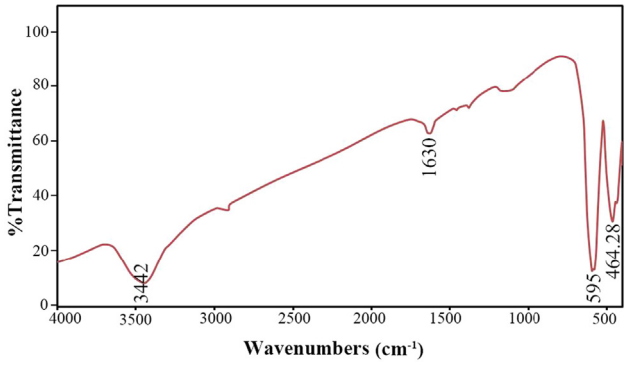

Fig. 8 Spectrum obtained from FT-IR analysis Tb_2CoMnO_6 nanoparticles sample No. 3.

Fig. 10, using Tauc's equation (Tauc et al., 1966), the estimated band-gap for these nanoparticles was calculated to be about 3.2 eV. The literature study confirmed this band-gap range for similar compounds such as 3.28, 3.4, 2.8, and 3.3 eV for Dy_2ZnMnO_6, Gd_2ZnMnO_6, Gd_2NiMnO_6, and Dy_2CoMnO_6 nanoparticles, respectively (Baladi et al., 2019; Orooji et al., 2020; Mohassel et al., 2020; Valian et al., 2017).

The efficiency of Tb_2CoMnO_6 nanoparticles in the photocatalysis process was investigated for the four organic dyes: Eriochrome black T, Rhodamine B, Thymol blue, and Acid red. The photocatalysis test was performed at ambient temperature under UV light for 90 min. Examination of the results showed a 70% discoloration for Eriochrome Black T in 90 min under UV light. For other dyes, 65, 38, and 22% discoloration was obtained from a solution containing Thymol blue, Acid red, Rhodamine B, respectively (Fig. 11). In general, in explaining the photocatalysis process with the help of

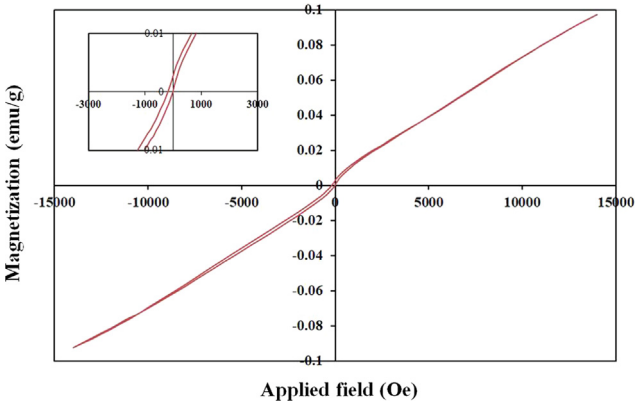

Fig. 9 Results of DRS analysis, and the inset shows estimated band-gap of Tb_2CoMnO_6 nanoparticles sample No. 3.

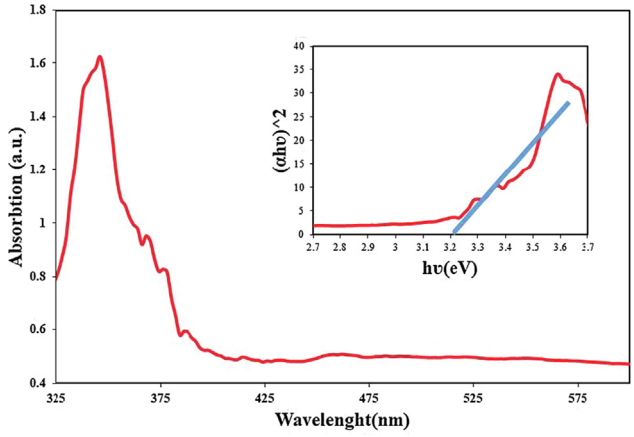

Fig. 10 Magnetization versus applied magnetic field at room temperature and the inset shows the magnified hysteresis loop of Tb_2CoMnO_6 nanoparticles sample No. 3.

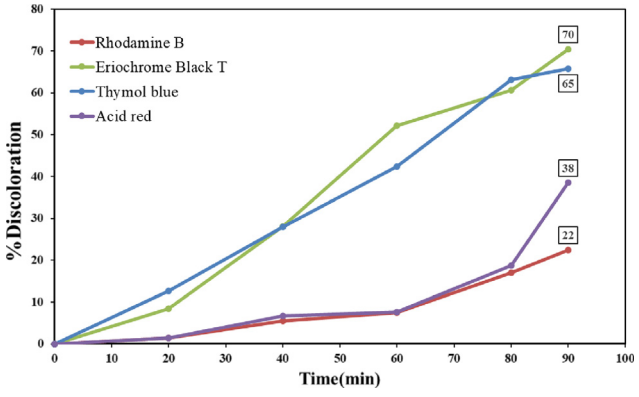

Fig. 11 Photocatalytic activity of Tb_2CoMnO_6 nanoparticles sample No. 3 under UV light.

semiconductor nanoparticles, the role of the electron-hole pairs caused by light radiation and electron transfer is discussed. Electron-hole pairs formed in the aqueous medium generate free radicals, which can be mentioned as follows

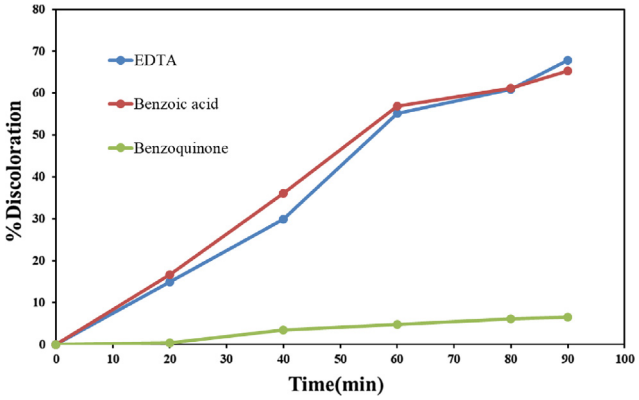

Fig. 12 Photocatalytic activity of Tb_2CoMnO_6 nanoparticles sample No. 3 in the presence of scavengers on discoloration Eriochrome Black T.

(Zhang et al., 2009; Raja et al., 2016; Zhang and Nosaka, 2014):

$$Tb_2CoMnO_6 + hv \rightarrow e^- + h^+ \quad (1)$$

$$e^- + O_2 \rightarrow O_2^- \quad (2)$$

$$h^+ + OH^- \rightarrow HO\cdot \quad (3)$$

$$2HO\cdot \rightarrow H_2O_2 \quad (4)$$

Which in interaction with organic dyes, degraded them, and discoloration is performed.

Scavengers were used to determine which radical species are effective in color degradation. Various compounds are used to trap free radicals (Schneider et al., 2020; Makama et al., 2020). 1, 4-Benzoquinone, EDTA, and Benzoic acid were used to remove superoxide, h^+, and hydroxide radicals, respectively. Therefore, photocatalysis test was performed in the presence of these materials for Eriochrome Black T under the same conditions. As shown in Fig. 12, the results showed that superoxide as a free radical produced in the photocatalysis process plays a significant role in the degradation of dye contamination in the presence of Tb_2CoMnO_6 nanoparticles. According to the results, the mechanism of the photocatalytic process can be considered as follows:

$$Tb_2CoMnO_6 \xrightarrow{hv} e^- + h^+ \quad (5)$$

$$e^- \xrightarrow{O^2} O_2^- \quad (6)$$

$$O_2^- + Organic\ contamin ant \rightarrow Destruction\ products \quad (7)$$

4. Conclusion

In summary, Tb_2CoMnO_6 double perovskite nanoparticles were synthesized by the sol-gel auto-combustion method for the first time. Different fuels were used to investigate the effect of fuel on particle size and morphology. Finally, the nanoparticles synthesized in the presence of maltose were selected as the optimal sample in terms of size and morphology. Various diagnostic and confirmatory analyzes were performed to eval-

uate the properties of nanoparticles. The estimated band-gap for these nanoparticles was calculated to be about 3.2 eV. Due to the observed appropriate optical properties, these nanoparticles were used as a potential candidate in water treatment in the photocatalytic process with the presence of different organic dyes. The photocatalysis process was performed for the four organic dyes: Eriochrome black T, Rhodamine B, Thymol blue, and Acid red under UV light; the highest discoloration was obtained for Eriochrome black T with 70%. The mechanism of the photocatalytic process was investigated with the help of various scavengers. The results showed that the path of discoloration of contaminants is done with the help of superoxide. In general, the results showed that these materials could be used in the photocatalysis process to remove dye contaminants, although further studies are needed to increase efficiency.

Declaration of Competing Interest

The authors declare that they have no known competing financial interests or personal relationships that could have appeared to influence the work reported in this paper.

Acknowledgment

The authors are grateful to the council of Iran National Science Foundation; (INSF, 97017837), and the University of Kashan for supporting this work by Grant No (159271/MD3).

References

Al-Mamun, M., Kader, S., Islam, M., Khan, M., 2019. Photocatalytic activity improvement and application of UV-TiO2 photocatalysis in textile wastewater treatment: A review. J. Environ. Chem. Eng. 7. 103248.

Assirey, E.A.R., 2019. Perovskite synthesis, properties and their related biochemical and industrial application. Saudi Pharmaceut. J. 27, 817–829.

Baladi, M., Soofivand, F., Valian, M., Salavati-Niasari, M., 2019. Sonochemical-assisted synthesis of pure Dy_2ZnMnO_6 nanoparticles as a novel double perovskite and study of photocatalytic performance for wastewater treatment. Ultrason. Sonochem. 57, 172–184.

Bhagwat, V., Humbe, A.V., More, S., Jadhav, K., 2019. Sol-gel auto combustion synthesis and characterizations of cobalt ferrite nanoparticles: Different fuels approach. Mater. Sci. Eng., B 248, 114388.

Chang, L., Li, J., Le, Z., Nie, P., Guo, Y.u., Wang, H., Xu, T., Xue, X., 2021. Perovskite-type $CaMnO_3$ anode material for highly efficient and stable lithium ion storage. J. Colloid Interface Sci. 584, 698–705.

Chaplin, B.P., 2019. The prospect of electrochemical technologies advancing worldwide water treatment. Acc. Chem. Res. 52, 596–604.

Dara, M., Hassanpour, M., Alshamsi, H.A., Baladi, M., Salavati-Niasari, M., 2021. Green sol–gel auto combustion synthesis and characterization of double perovskite Tb_2ZnMnO_6 nanoparticles and a brief study of photocatalytic activity. RSC Adv. 11 (14), 8228–8238.

Garcia-Muñoz, P., Lefevre, C., Robert, D., Keller, N., 2019. Ti-substituted $LaFeO_3$ perovskite as photoassisted CWPO catalyst for water treatment. Appl. Catal. B: Environ. 248, 120–128.

George, J., Halali, K.V.V., C. G., S., Suvina, V., Sakar, M., Balakrishna, R.G., 2020. Perovskite nanomaterials as optical and electrochemical sensors. Inorg. Chem. Front. 7 (14), 2702–2725.

Gomes, S.D.C., Zhou, J.L., Li, W., Long, G., 2019. Progress in manufacture and properties of construction materials incorporating water treatment sludge: A review. Resour. Conserv. Recycl. 145, 148–159.

Hassanpour, M., Salavati-Niasari, M., Safardoust-Hojaghan, H., 2021. Sol-gel synthesis and characterization of Co_3 O4/CeO_2 nanocomposites and its application for photocatalytic discoloration of organic dye from aqueous solutions. Environ. Sci. Pollut. Res. 28 (6), 7001–7015.

Hassanpour, M., Tafreshi, S.A.H., Salavati-Niasari, M., Hamadanian, M., 2021. Toxicity evaluation and preparation of $CoWO_4$ nanoparticles towards microalga Dunaliella salina. Environ. Sci. Pollut. Res. 28 (27), 36314–36325.

Huang, S., Xu, Y., Xie, M., Xu, H., He, M., Xia, J., Huang, L., Li, H., 2015. Synthesis of magnetic $CoFe_2O_4$/g-C_3N_4 composite and its enhancement of photocatalytic ability under visible-light. Colloids Surf., A 478, 71–80.

Iglesias, M.-C.-A., 2020. A review of recent advances and future challenges in freshwater salinization. Limnetica 39, 185–211.

Jung, H.S., Park, N.-G., 2015. Perovskite solar cells: from materials to devices. Small 11 (1), 10–25.

Koe, W.S., Lee, J.W., Chong, W.C., Pang, Y.L., Sim, L.C., 2020. An overview of photocatalytic degradation: photocatalysts, mechanisms, and development of photocatalytic membrane. Environ. Sci. Pollut. Res. 27, 2522–2565.

Makama, A., Salmiaton, A., Choong, T., Hamid, M., Abdullah, N., Saion, E., 2020. Influence of parameters and radical scavengers on the visible-light-induced degradation of ciprofloxacin in ZnO/SnS_2 nanocomposite suspension: Identification of transformation products. Chemosphere 253, 126689.

Mitzi, D.B., 2019. Introduction: perovskites. Chem. Rev. 119, 3033–3035.

Mohassel, R., Amiri, M., Abbas, A.K., Sobhani, A., Ashrafi, M., Moayedi, H., Salavati-Niasari, M., 2020. Pechini synthesis using propylene glycol and various acid as stabilizing agents and characterization of Gd_2NiMnO_6 ceramic nanostructures with good photocatalytic properties for removal of organic dyes in water. J. Mater. Res. Technol. 9 (2), 1720–1733.

Mukhopadhyay, R., Bhaduri, D., Sarkar, B., Rusmin, R., Hou, D., Khanam, R., Sarkar, S., Biswas, J.K., Vithanage, M., Bhatnagar, A., 2020. Clay–polymer nanocomposites: Progress and challenges for use in sustainable water treatment. J. Hazard. Mater. 383, 121125.

Natalia, P., Silvia, F., Silvina, S., Miguel, P., 2020. Climate change in northern Patagonia: critical decrease in water resources. Theor. Appl. Climatol., 1–16

Orooji, Y., Mohassel, R., Amiri, O., Sobhani, A., Salavati-Niasari, M., 2020. Gd2ZnMnO6/ZnO nanocomposites: Green sol-gel autocombustion synthesis, characterization and photocatalytic degradation of different dye pollutants in water. J. Alloys Compounds. 155240.

Raja, V., Shiamala, L., Alamelu, K., Ali, B.J., 2016. A study on the free radical generation and photocatalytic yield in extended surfaces of visible light active TiO_2 compounds. Sol. Energy Mater. Sol. Cells 152, 125–132.

Rodríguez-Carvajal, J., 1993. Recent advances in magnetic structure determination by neutron powder diffraction. Physica B 192, 55–69.

Samanta, A., Goswami, M.N., Mahapatra, P.K., 2018. Optical properties and enhanced photocatalytic activity of Mg-doped ZnO nanoparticles. Physica E 104, 254–260.

Sariful Sheikh, M.d., Ghosh, D., Dutta, A., Bhattacharyya, S., Sinha, T.P., 2017. Lead free double perovskite oxides Ln_2NiMnO_6 (Ln = La, Eu, Dy, Lu), a new promising material for photovoltaic application. Mater. Sci. Eng., B 226, 10–17.

Schneider, J.T., Firak, D.S., Ribeiro, R.R., Peralta-Zamora, P., 2020. Use of scavenger agents in heterogeneous photocatalysis: truths, half-truths, and misinterpretations. Phys. Chem. Chem. Phys. 22 (27), 15723–15733.

Shirazi, P., Rahbar, M., Behpour, M., Ashrafi, M., 2020. La_2MnTiO_6 double perovskite nanostructures as highly efficient visible light photocatalysts. New J. Chem. 44 (1), 231–238.

Silva, R.X., Almeida, R.M., Moreira, R.L., Paniago, R., Rezende, M. V.S., Paschoal, C.W.A., 2019. Vibrational properties and infrared dielectric features of Gd_2CoMnO_6 and Y_2CoMnO_6 double perovskites. Ceram. Int. 45 (4), 4756–4762.

Sivasamy, R., Venugopal, P., Espinoza-González, R., 2020. Structure, electronic structure, optical and magnetic studies of double perovskite Gd2MnFeO6 nanoparticles: First principle and experimental studies. Mater. Today Commun. 25. 101603.

Tauc, J., Grigorovici, R., Vancu, A., 1966. Optical properties and electronic structure of amorphous Germanium. Phys. Status Solidi (b) 15 (2), 627–637.

Valian, M., Beshkar, F., Salavati-Niasari, M., 2017. Urchin-like Dy_2CoMnO_6 double perovskite nanostructures: new simple fabrication and investigation of their photocatalytic properties. J. Mater. Sci.: Mater. Electron. 28, 12440–12447.

Wu, Z.-Y., Ma, C.-B., Tang, X.-G., Li, R., Liu, Q.-X., Chen, B.-T., 2013. Double-perovskite magnetic La2NiMnO6 nanoparticles for adsorption of bovine serum albumin applications. Nanoscale Res. Lett. 8, 1–4.

Zhang, H., Millington, K.R., Wang, X., 2009. The photostability of wool doped with photocatalytic titanium dioxide nanoparticles. Polym. Degrad. Stab. 94, 278–283.

Zhang, J., Nosaka, Y., 2014. Mechanism of the OH radical generation in photocatalysis with TiO_2 of different crystalline types. J. Phys. Chem. C 118, 10824–10832.

Zhu, D., Zhou, Q., 2019. Action and mechanism of semiconductor photocatalysis on degradation of organic pollutants in water treatment: A review. Environ. Nanotechnol., Monitoring Manage. 12. 100255.